
ISSN: 2321-2152
IJMECE
International Journal of modern
electronics and communication engineering
E-Mail
editor.ijmece@gmail.com
editor@ijmece.com
www.ijmece.com

ISSN2321-2152www.ijmece .com

Vol 5, Issuse.3July 2017

3D printing of mechanically competent polycaprolactone-reduced polycaprolactone scaffolds made from graphene oxides

Aamer Sohail[1] , Meer Mustafa Ali[2], Touseef Ahmed[3],

ABSTRACT:

Scaffold manufacturing has benefited from 3D printing's capacity to manufacture structures with fine control over bulk geometry and interior design. Engineers are always looking for new ways to create scaffolds for various tissues. During this study, we developed 3D-printed parts.polycaprolactone (PCL) with varying quantities of reduced graphene (RG) composite scaffoldsRGO at 0.5, 1, and 3 wt%.%. A two-step manufacturing procedure was used to provide an evenThe PCL matrix is mixed and distributed with rGO sheets. Preparation of the inks was done by generatingconcoctions of PCL and rGO evaporation castings that were then put into the reactorExtrusion 3D printing. The resulting scaffolds were 3D printed with excellent resolution and flawlessly incorporated.consistency and fidelity in all groupings. This, along with the rGO's uniform distribution, provides compelling evidence.compressive strength and stiffness of the polymer matrix were greatly enhanced byAt 0.5 wt. % rGO incorporation, 185 percent and 150 percent, respectively, were achieved. The scaffolds' in vitro reaction wasstem cells generated from human adipose tissue. Cellular compatibility and support were found in all scaffolds.growth and viability of the cell. Biologically compatible, mechanically strengthened, and 3D manufactured PCLrGOs.In the field of regenerative engineering, scaffolds hold great promise.

INTRODUCTION

These three-dimensional constructions, known as scaffolds, are temporary templates that let cells grow and regenerate tissue in the correct environment. There are a number of considerations that need to be taken into account while designing these temporary templates. Physical abuse should not be a problem for them.in order to carry out their primary function of supporting the structure of the building.To allow for tissue renewal. They need to be safe and biocompatible. They should be able to sustain themselvesis the process through which cells attach to one another and spread outward. They are expected to deteriorate with time.

In addition, they produce byproducts that are completely safe for the human body. Additionally, they must be very permeable and breathable.feature a network of linked pores that aids in cell development and metabolic waste transfer Scaffolds may be made using a wide range of processes, including solvent casting5.castings are frozen6. freezedrying7,electro spinning8,foam9, gas in the form of melt molding11, particulate-leaching10 phase change12and the ability to assemble one self 13 approaches, such as sol–gel However, inadequate scaffold control is a major drawback for most approaches. design, architecture, pore network, and pore size are all aspects of pore network design. In addition, the scope of these methods is limited. make scaffolds with the same design characteristics consistent and repeatable15,16.It is a cutting-edge technique that may be used to create complicated objects, such as automobiles, using 3D printing.high-precision, precisely controlled geometries.

Assistant Professor and Head[1], Assistant Professor[2,3]
Dept. of Mechanical Engineering,
Global Institute of Engineering and Technology, Moinabad, Hyderabad

Layer-by-layer deposition is used to build structures.successive layers are fused together to form the final structure. The constraints of 3D printing are no longer an issue.scaffold fabrication approaches typical in that they can generate well specified and controlled designsas well as in terms of their outside shape and interior architecture, strand size, and pore size and location.Inkjet printing, laser-assisted printing, and extrusion printing are the three most common 3D printing production processes, each with distinct benefits. 17.3D printing based on extrusiona large range of materials may be printed using the printing process, which is the most adaptable.

Polymers, ceramic pastes, hydrogels, and bioinks infused with living cells are all examples of this class of materials. It has a high degree of accuracy and fidelity20.that both areBased on the substance being used and the procedure used to solidify it17,20.PLGA (poly(lactic-co-glycolic acid)), PLA, and other biodegradable synthetic polymers, such asDue to its biocompatibility, polycaprolactone (PCL) is one of the most often utilised polymers for scaffold production.biodegradability, ease of processing, and a wide range of mechanical qualities21.Particularly PCL is FDA-approved.synthetic polyolefin that may be cheaply synthesised and processed to be used in an array ofapplications22.

This material's extended breakdown time may be utilised to make biodegradable gadgets for long-term usage.may also be adjusted to control the pace at which the polymer degrades23.PCL is highly soluble and easily processed.many organic solvents, making it ideal for a wide range of manufacturing methods. [page needed]include a variety of tissues21.Furthermore, it has a melting temperature of 60 °C and a glass transition temperature of 60 °C.Extrusion-based 3D printing uses this polymer because of its high melting point (55–60 °C).DespiteBut the hydrophobicity and absence of functional groups in PCL pose significant barriers to its potential.Applied to biomedical researchCarbon atoms are densely packed into a two-dimensional honeycomb pattern to form graphene, a single atomic layer.Its large specific surface area and exceptional mechanical, electrical, thermal, and optical qualities make it a must-have for every engineer or scientist.It's one of the most adaptable materials when it comes to a variety of industries and uses. Awe-inspiring featuresgraphene and the graphene family of materials (GFMs) are a growing area of study and research in the scientific community.among the world's scientists25–There are two types of graphene oxide (GO): oxidised graphene and unoxidized graphene.the process of graphite oxidation and exfoliation. Despite the fact that oxygen functional groups are introduced during the oxidation process,Defects in graphene's planar structure due to its hydrophilicity and ease of processing reduce its properties.properties28,29.Graphene was decreased in order to eliminate oxygen functional groups that interfere with the structure.

When GO is reduced, an oxide (rGO) is formed. rGO is a structure that lies somewhere in betweenthe ideal graphene sheet and the oxidised GO structure with some of its characteristics partially restoredthat were oxidized30 and hence lost.In most cases, the physical and chemical properties of rGO-polymer composites are improved.as well as biological characteristics31–Filling up PCL-based scaffolds with rGO enhances the structural properties, such as stiffness and strength.constructions that are more capable and suited mechanically because of the strength and toughness of the scaffoldsas a means of supporting weight32,33.When it comes to hydrophilicity, the rGO's physical and chemical features helpproteins and growth factors that can be absorbed by scaffolds33,34.Aside from that, the inclusion of rGOboostscell adhesion, spread, and proliferation substrates. Notice the rGOThe inclusion of progenitor and stem cells into specific lineages may aid in their differentiation, which is particularly important.Biomaterials for tissue regeneration are critical32,34,35.

This study examined the impact of rGO on 3D printed PCL-rGO composite scaffolds.altering the composite scaffolds' characteristics Extrusion-based additives were used to create the scaffolds.It allowed us to create complex, high-resolution structures. We integrated a variety ofassess their printability and their rGO content inside the 3D printed scaffoldsBiological, mechanical, and structural characteristics. We show that the inclusion of rGO may improve3D printed scaffolds may be physically reinforced and the mechanical characteristics of PCL can be improved at the same time.The printing technique and the biocompatibility of the final composite structures are unaffected.**Results and discussion**3D printing and ink preparation. Figure 1 depicts a simplified flowchart of the different scaffolding preparation procedures. A two-step approach was used to achieve a uniform distribution of the rGO filler in the 3D printing inks and scaffolds created by the process of 3D printing The inks for 3D

printing were made using this method.film casting using solvent evaporation. It was possible to produce homogeneous composites in the laboratory using this method.avoid the need to raise temperature before to 3D printing by reducing the temperature. PCL-rGOCompoundsIn advance, we created and then cut into films with varying concentrations of rGO (0, 0.5, 1, and 3 weight percent).

The 3D printer's high-temperature cartridge was loaded with smaller pellets.The prepared inks were first 3D printed to provide an exact and uniform pattern between the scaffolds.Smaller cylindrical scaffolds were then cut from the bigger constructions. a 60-degree change between the next twolayering resulted in a structure with linked pores. The 0/60/120 lay-down pattern has a 60° angle.has been shown to have an excellent adhesion support in the form of a patterncellular proliferation and viabilityMoreover, we havemechanical qualities that are superior41that are not affected by the loading direction and are anisotropic42.The 3D printed scaffolds are characterised in terms of their shape. Figure 2 shows the SEM and photomicrographs.photographs showing several rGO-loaded 3D printed scaffolds. Figure 2a and video S1 (more information)how composite inks are deposited and 3D printed things are built layer-by-layerthat had been shaped into cylindrical scaffolds. Fig. 2b and c show the top and side views of the same object.consistency of the printing process and strand homogeneity across scaffolds The view from the summit is 50 degrees.A 60° change in the pattern is visible, as are the resulting linked pores, which all have the same size and form.An interlocking polymer matrix covers the rGO molecules and is smooth, dense and continuous. There's aat the juncture between the next two strands, the neighbouring layers merge seamlesslyas well as 50-degree side-view views), assuring the scaffolds' ability to adequately support and transfer loads.The high-magnification images also show no clumping or aggregation of the polymer or rGO.

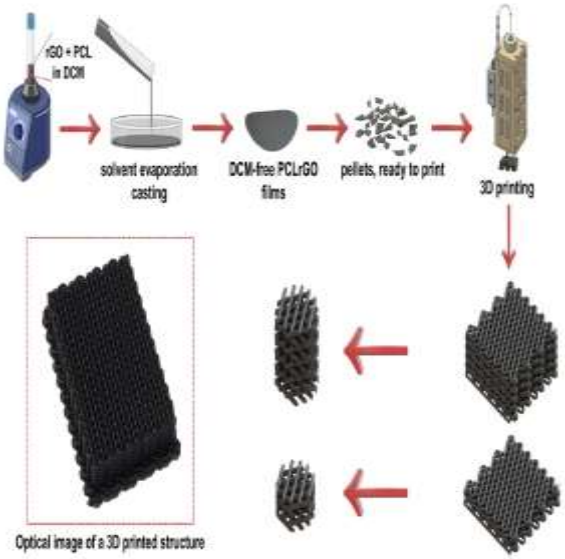

FIG 1: To make the PCL-rGO 3D printed scaffolds, follow the steps in Figure 1. A homogeneous dispersion of PCL/rGO was first produced using vortexing. The solution was allowed to evaporate before the suspension was cast into films. They were then lyophilized and chopped into smaller pieces.additive manufacturing 3D printer cartridge pellets. High-temperature 3D printing produced structures with varying wall thicknesses.followed by being punched into scaffolds for further testing. The finished 3D model as seen via a lens. The construction of a printed PCL-rGO printer is shown.

SEM photos of the rGO sheets dispersed in the PCL matrix as a result of the solvent evaporation casting procedure.New tissue formation is guided by the interior structure of scaffolds, which are vital for cell activities.formation. As a result, the porosity of a specific scaffold influences seeding and penetration as well as distribution and penetration.the development of cellsFor each scaffold, we calculated average strand diameter and pore diameter (Fig. 3). TheoreticalIn the CAD programme SolidWorks, values signify those that have been specified prior to printing. The results of the testsSEM pictures of the printed scaffolds were processed using an ImageJ macro code. AsStrand diameter and pore size are identical across all scaffold groups, as illustrated in Figure 3c, suggesting.

The varied amounts of rGO do not influence the printed structures. The capacity to alter the design of a buildingBy just altering the printing settings, it is essential to create composite 3D printed scaffoldsHigh-quality, repeatable and consistent fabrication of structures.The theoretical values and the observed values for the strand diameter were somewhat different.as well as the size of the pore. A total of 324.95 1.95 m was found to be the average diameter of the strands in all groups.More than 24.95 m bigger than the theoretical value. The inks' die-swelling causes a rise in strand diameter.A

characteristic of viscoelastic polymer inks is their tendency to expand upon extrusion from the nozzles44,45.TheWe found that the observed average pore size was roughly 24.83 m less than its estimated theoretical average size (395.17% 84.11%).value. Secondary to and almost equivalent to strand diameter growth, the pore size reduction indicates that the strands are becoming longer.precision (resolution less than one micrometre) in printing. It's crucial that the pores in the network be linked.Tissue in growth and vascularization, particularly in bone, benefit from a range of 400 m.tissue of cartilage46, 47.The 3D printed scaffolds' material properties. Analysis of the thermogravimetric data was performed.Make sure to look at the 3D printed scaffolds for rGO content and their composition. This was the first time I'd ever heard ofBecause PCL and rGO degrade at different temperatures, this is a possibility.

All scaffolds' TGA curves areExamples of this may be seen in figure 4. Between 300 and 450 °C, PCL's mass begins to decline sharply, indicating a structural change.The polymer breaks down. All composite PCL-rGO samples showed a significant mass decrease.It reflects the fact that PCL is a significant component of the composites. The remaining mass after 450 degrees Celsiusconstant and directly proportional to the concentration of reverse transcriptase (rGO) in samples (Fig. 4b).We utilised X-ray powder diffraction to examine the scaffolds in more detail (Fig. 4d).As seen in Figure 1, the PCL has two distinct peaks, which may be found at 2 = 21.9° (plane 1) and 2 = 23.5° (plane 2)respectively48.The existence of these two peaks was found in all of the 3D printed scaffolds.Samples all included semi-crystalline polymers. The typical rGO peak is located at 2 = 26.16°, which is equivalent to49-degree angle of attackIn spite of the fact that rGO was used at a lower concentration in the composites, it still had a significant impact.

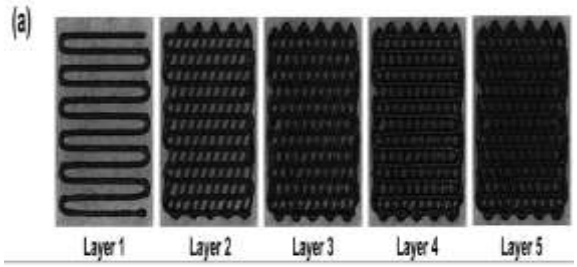

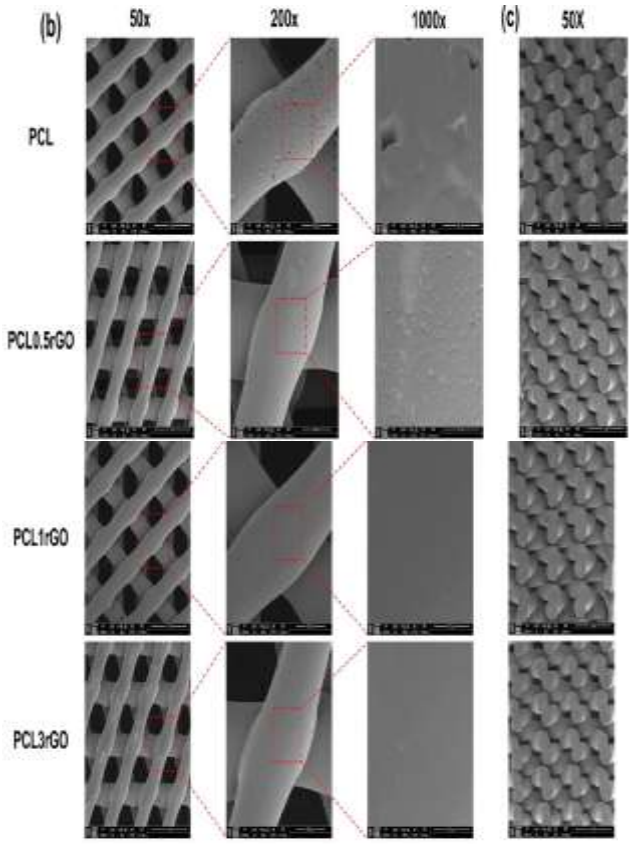

Figure 2 demonstrates this concept. Scaffolds' morphological assessment. (a) 3D printer CCD camera images of the each layer that is deposited during printing. picture acquired using a scanning electron microscope (SEM) of 3D printed scaffolds (b)view from above (a) with varying magnifications (b) and view from the cross-section (c)However, even in PCL3rGO,

where rGO had a lower peak intensity than PCL, a clear peak could be seen.The wettability and hydrophilic/hydrophobic properties of many materials have been studied using static contact angle measurements.samples' characteristics (Fig. 5a and Supplementary video S2). It was found that PCL's water contact angle wasHydrophobicity is indicated by a reading of 87.4°. The water contact angle was lowered by the addition of rGO. ThererGO increased in tandem with a reduction in water contact angle, which was measured at 82.7°.

A significant difference in PCL0.5rGO's molar mass from PCL1rGO's and PCL3rGO's molar massthroughout all the study groups. The capacity of rGO and GFMs to promote substrate hydrophilicity is a unique property of both compounds.biocompatibility of graphene-based materials has been shown to be affected by this well-established and well accepted property.and their effects on cells38,50–54.The PCL-rGO scaffolds may be used in regenerative engineering applications if more testing is done.Their ability to decompose was

examined. Simulated bodily fluid (SBF) was used to incubate the scaffolds.a 14-day period in which their swelling percentage and weight loss were monitored under physiological settingsThe percentages that were calculated were noted (Fig. 5b,c). As with contact angle measurements, there has been an upward tendency inThe swelling rate of the PCL-rGO scaffolds increased when rGO was added at all concentrations.Scaffolding made of bare PCL The percentage increase in swelling rate was directly related to the amount of rGO in the product.As a function of time, the PCL3rGO scaffolds exhibited the largest water absorption (Fig. 5b). TheScaffold weight loss % correlated with the findings of contact angle measurements, as welland the pace at which the scaffolds swell. The PCLrGO saw a rise in the proportion of weight reduction.the incubation duration and rGO concentration of the scaffolds were inversely proportional (Fig. 5c).

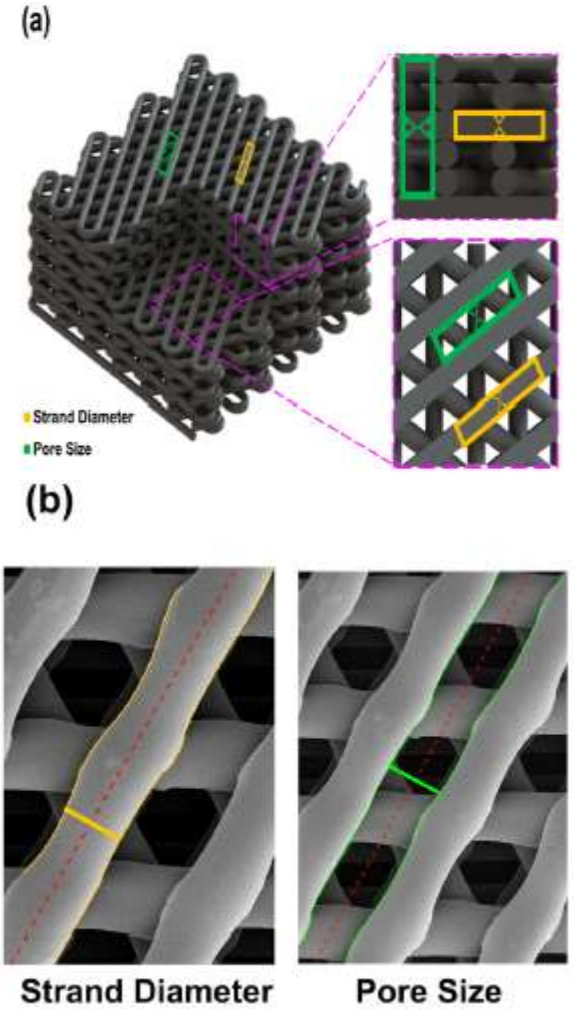

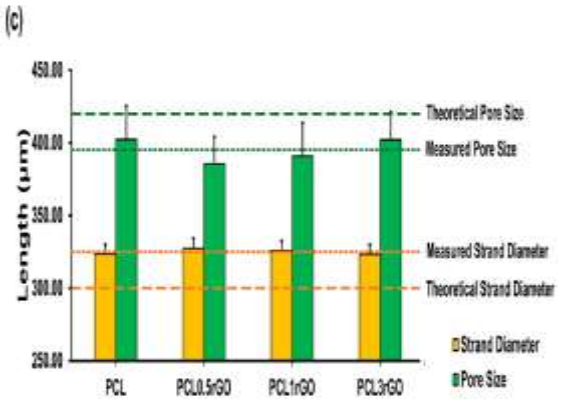

Fig 3 : From two perspectives, printed structures depicting the structural pattern, the strand diameter, and pore size (b) An illustration of the ImageJ macro code's measuring method. The yellow lines indicate the strands' boundaries, whereas the green lines denote the pore regions' boundaries. The red dashed lineeach strand or pore area's average angle Representational: The yellow or green perpendicular lineThe strand diameter or pore size may be determined by measuring the line's breadth. In (c), the results of the measurementswith relation to their respective theoretical values, strand and pore diameters. The following are the findings:the average is less than the standard deviation.

Tosummarise, the incorporation of rGO enhanced hydrophilicity, increased water absorption and swelling, and sped up degradation of the PCL-rGO composite scaffolds.

Mechanical evaluation of the 3D printed scaffolds: Mechanical testing of the 3D-printed scaffolds is performed.. Measurement of a machine's performance mechanicallyusingrGO-incorporation in 4 mm thick, 4-millimeter diameter scaffolds to study the impact of rGOA single-compression test was carried out. There are several stress–strain curves for the different scaffolds shown in Figure 6.Compressive moduli and strengths have been computed. Stiffness-strain curves were comparable across scaffolds under the same stress-strain conditions.loading. A linear elastic or Hookean area precedes a plateau, which is followed by a second plateau.densely populated zone. The deformation behaviour of did not change when rGO was added at a concentration of 0.5–3 weight percent.Theframeworks.

Mechanical properties improved the most when rGO at 0.5 weight percent was added, as seen in Fig. 6b,c.properties. The compressive modulus and compressive strength of the improved significantly.Scaffolds made of PCL0.5rGO. The compressive modulus and tensile strength of the PCL0.5rGO scaffolds are superior to those of the PCL scaffoldsStructural integrity was improved by 150% and 185%. It's possible to increase the rGO

content from 0.5% to 1%.or 3% of the scaffolds' weight decreased their mechanical characteristics, resulting in decreased mechanical performance.The processes behind the scaffolds' enhanced mechanical characteristics at 0.5 weight percent rGO were examined.structure at the subnanometer level using wide-angle x-ray scattering (WAXS) (Fig. 7). PCL has two of them on exhibit.Its crystalline structure is thought to be responsible for the substantial peaks at 2 = 22.5° and 2 = 25°. The defining featureAn interlayer distance (0 0 2) peak in graphite or aggregated graphenic layers (d-spacing)between the sheets lies at a distance of about 2 = 27°55,56. this peak in PCL0.5rGO and its lack in PCL0.5RGO sheets are being re-stacking in PCL1rGO and PCL3rGO, and this is shown by their existenceOnly at the higher rGO loading doses in these samples is this seen, while at lower loading values of 0.5.

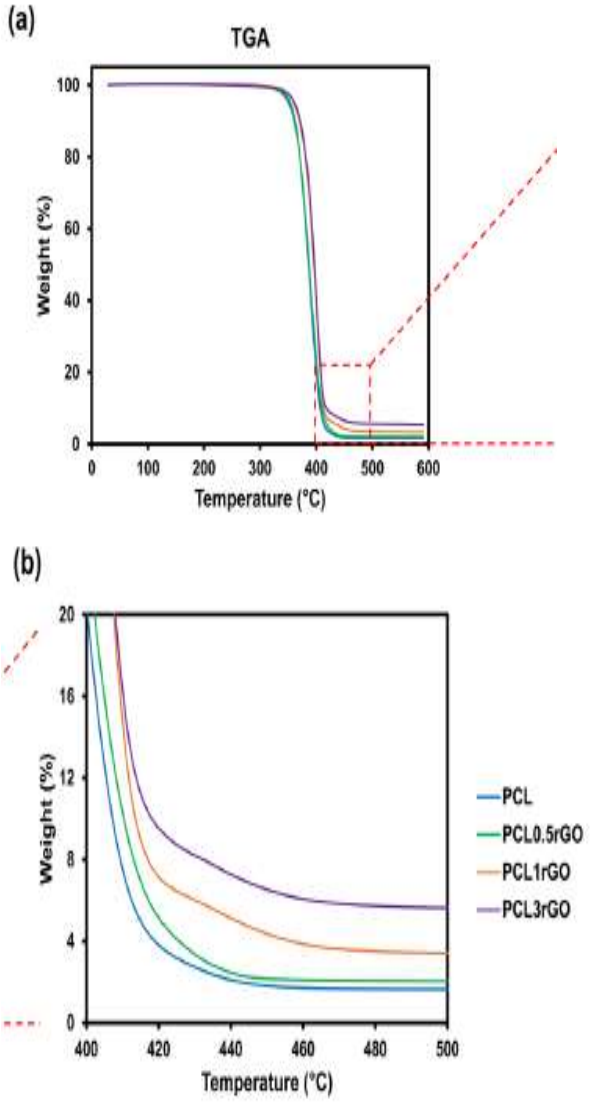

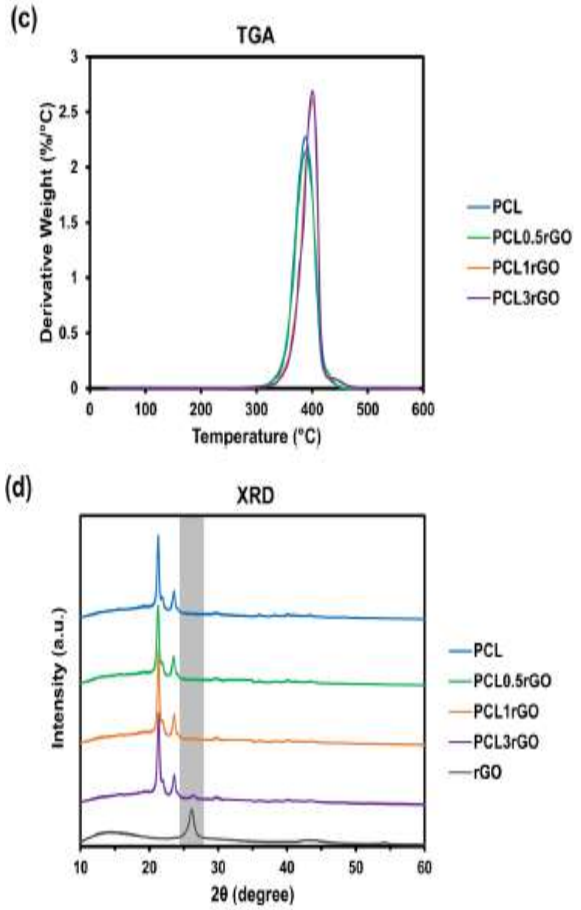

FIG 4 : A characterisation of the 3D-printed scaffolds' composition is shown in Figure 4. Thermal images of the 3D-printed scaffolds created using TGA. (b) TGA thermograms showing the residual mass of each sample in the expanded area. First derivative TGA curves of the 3D printed scaffolds. Non-porous 3D XRD patterns rGO and printed scaffolds.TherGO sheets are exfoliated and disseminated in the polymeric matrix at a wt. percent level.

Interfacial contacts between rGO sheets and polymer chains are strengthened by their inherent strength, high specific surface area and homogeneous dispersion within the polymer matrix.so that stress may be transferred efficiently between the two of them, leading to behaviours that reinforce one another.

In the PCL0.5rGO composites, this may be seen. Excessive use of the rGO filler in PCL1rGO and PCL2rGOrGO sheets re-stack under the influence of PCL3rGO, resulting in irreversible aggregates that obstruct the effective flow of information.of weight and degrade the scaffolds' mechanical properties57,58..High-modulus GFMs in low-modulus polymer matrices may have a considerable impact on the mechanical properties.in composite constructions' mechanical characteristics. GFMs'

polymer-reinforcing effectsMatrix structure is determined by the graphene, the polymer matrix, and the composite material.how the graphene filler disperses inside and interacts with the matrix, as well as the technique of preparationInAdditionally, the structural and physicochemical features of the composite may be found in 3D printed scaffoldsPore size, surface area, and strand diameter all have an essential impact in the composition of materials50,60.WhileAccording to the majority of research, scaffolds and other constructions using GFMs have improved mechanical properties.performance51,61–65, a few research have showed that adding rGO to the mix has no effect on the outcomes.detrimental impact on the mechanical performance of the constructions35,66..Between research, there are a lot of differences.

Variations in all the components of our 3D printed structures are likely to be responsible for the mechanical improvements we have noticed.both the aforementioned criteria and the various geometrical characteristics. Consistency in strand length is critical.across distinct PCL-rGO scaffolds (Fig. 3), no matter how much or how little rGO is presentBecause of the presence of PCL0.5rGO in the scaffolds, the mechanical performance of the PCL0.5rGO scaffolds is increasednot because of any geometrical properties, but because of rGO Beyond the two-stage manufacturing procedure,bigger strand diameters and smaller pore sizes were used to create seamless scaffolds.increase mechanical performance as well. Finally, the exfoliated rGO was uniformly dispersed.in the polymer matrix are crucial to the effective passage of loads and the reinforcing effects that areThis was most clearly shown in PCL0.5rGO.Finally, to see whether treating PCL by film casting influenced its mechanical characteristics, the experiment was conducted.

A comparison was made between the elastic moduli of 3D printed scaffolds created using film-casted PCL pellets and thoseraw PCL pellets were used in the production of these products. The scaffolds differed little from one another.showed that the ink-processing procedures (Supplementary Fig. S1) could be used for either printing techniqueThe mechanical characteristics of the PCL printed structures were unaffected by pretreatment.

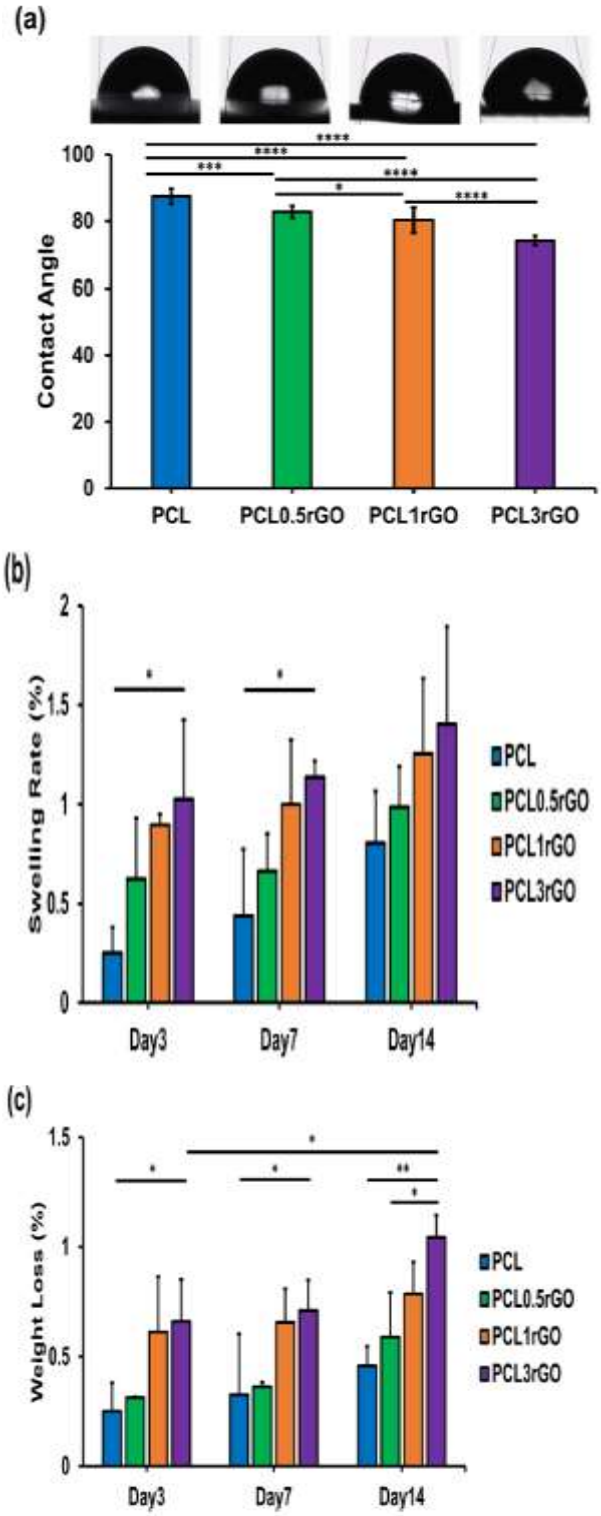

FIG 5 : ***In vitro biodegradation behaviour and hydrophilicity of the scaffolds are shown in Figure 5. Scaffolds with varied concentrations of rGO are shown in (a) contact angle photos and measurements. n = 5 gives us a mean standard deviation. 3D-printed scaffolds (b,c) following in vitro degradationA 14-day incubation of SBF under physiological conditions. (b) the rate of growth and (c) (c)Scaffold weight loss reported in percent and***

provided as mean and standard deviation (n=3)A 0.0001-percent chance of this finding being correct was used.

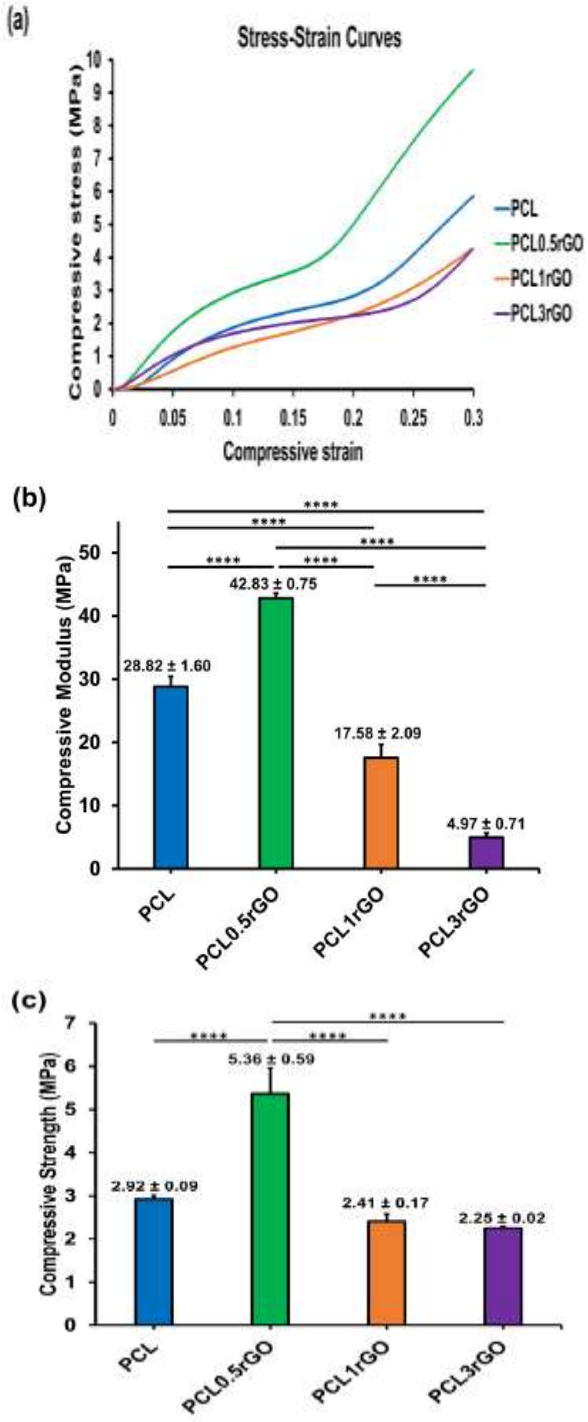

*Figure 6. Mechanical analysis of the 3D printed scaffolds. (a) The representative stress–strain curves of the 3Dprinted scaffolds under uniaxial compression loading. (b) The compressive moduli and (c) compressive strengthof the 3D printed scaffolds. Results are presented as mean ± SD (n = 4) (****p < 0.0001).*

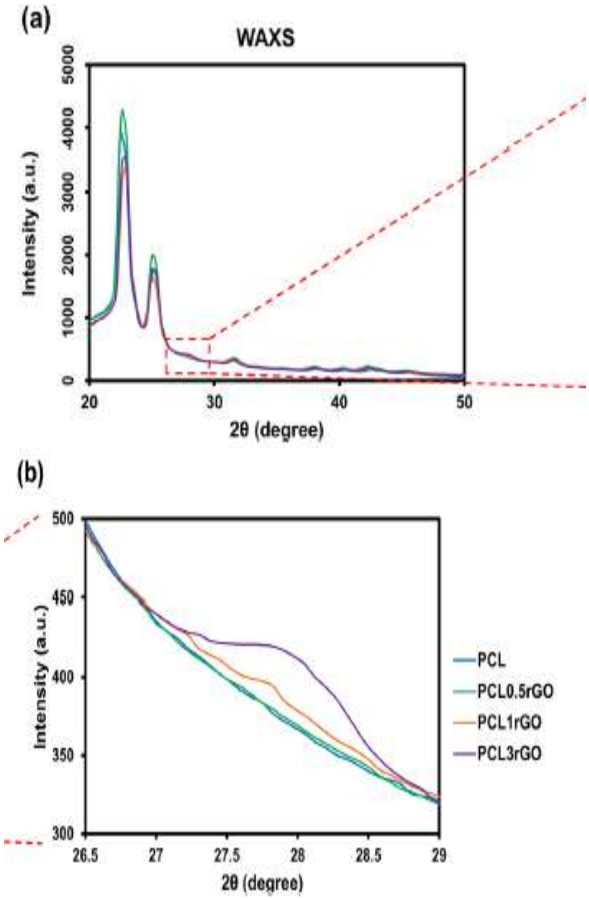

Figure 7. Sub-nanometer level structural analysis of the 3D printed PCL-rGO scaffolds. (a) The WAXS patternsof the 3D printed scaffolds. (b) The enlarged region of the WAXS pattern indicating the characteristic peak ofgraphite which corresponds to the aggregation and re-stacking of the graphenic layers.

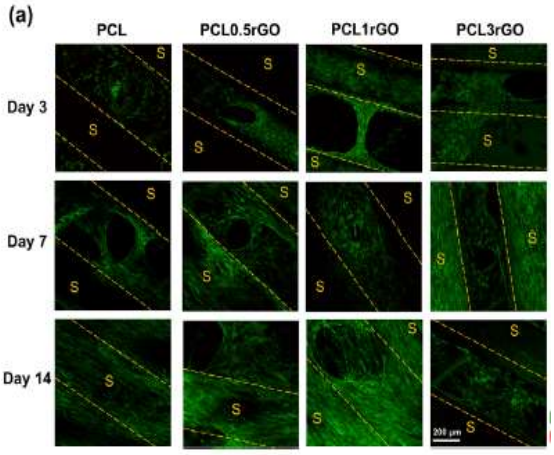

(b)

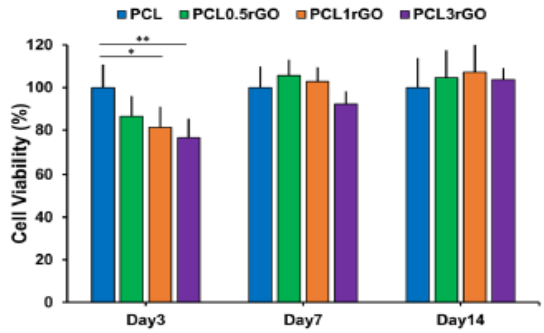

Figure 8. Cytocompatibility of the 3D printed scaffolds. (a) Representative confocal micrographs of hADSCsgrown on the 3D printed scaffolds and stained with the fluorescent live/dead assay (green, calcein AM; red,ethidium homodimer-1). The strand borders are identified using dashed lines (scale bar 200 µm). (b) Cellviability of hADSCs on the 3D printed scaffolds, measured by the MTS assay. Results are expressed as % viabilitywith respect to the PCL control at each time point and are presented as mean ± SD (n = 3) (*p < 0.05, **p < 0.01).

In vitro evaluation of the 3D printed scaffolds: The 3D printed scaffolds were tested in a lab environment. For tissue and regenerative engineering, the biocompatibility of the scaffolds and their ability to promote cell adhesion and growth are critical. These scaffolds were tested for their cytocompatibility, as well as the effect of rGO inclusion, on cell viability.stem cells generated from human adipose tissue (hADSCs). The scaffolds were seeded with cells, and cells were seeded at predetermined intervals.MTS cellular proliferation test and live/dead assay dye were used to examine time points.There are confocal pictures for days 3, 7, and 14 of the cell-seeded scaffolds shown in Figure 8a. Therescaffolds of all compositions have good cell viability with little to no cell death. The use of all scaffolds contributed to the success of the project.HADSC adhesion and growth, no matter what rGO content. To my surprise, including rGO proved to boostAt a larger degree than the PCL scaffolds, cell development and proliferation The PCL0.5rGO and the PCL1rGO are two such variants.cell coverage was larger on the scaffolds, as well as the 3D printed strands and pores between them.Supplementary Fig. S2 is shown in Figure 8a. In addition, the strands had more cellular bridging between them, resulting in a stronger connection.Indicating their higher ability to support cell growth.The number of hADSCs and their rate of proliferation on the 3D printed scaffolds could also be measured utilisingControls include the MTS proliferation test and PCL scaffolds (Fig. 8b). There was a notable reduction inconcentration-dependent number of cells on composite scaffolds at day 3 after seeding. This is just what I was looking for.Due to the PCL-rGO scaffolds' increased hydrophilicity compared to PCL scaffolds, which on the other hand are less hydrophilic.Initial cell seeding allows the cell droplets to pass through the scaffolds and onto the well plates once they have been injected.unlike the more hydrophobic PCL scaffolds, which keep droplets clinging to their surface,making sure that the cells have enough time to connect to the substrates At day 7, however, the PCL-rGO cells showed signs of ageing.The proliferation of composite scaffolds had made up for the original cell shortage. There was a small increase in the number of people in attendance.days 7 and 14, there was a trend in the proportion of viable cells, but no significant difference was seen at any of these pointstime interval between any two research teams.The physicochemical properties (size, shape, surface) of GFMs influence their biocompatibility.chemistry), medium, dosage, and duration of exposure, as well as the kind of cell involved25,27.According to the majority of research, this is true.The biological performance of scaffolds may be improved by including modest quantities of GFMs.67–69.An increase in protein absorption and wettability are all made possible by the GFMs.Certain lineages are formed via adhesion, proliferation, and differentiation. The – stacking and the non-covalentThe large specific surface area and presence of oxygen functional groups in rGO allow for the highcellular adhesion, spreading, and proliferation are all made easier by protein density loading and adsorption70.On the PCL-rGO scaffold, cell adhesion and viability and growth of hADSCs were maintained.gives proof of the substrates' biocompatibility. All of the measured concentrations of rGO had a positive effect.did not have any negative impact on human tissues or cells when administered.

Conclusion

Our 3D printed PCL-rGO scaffolds have been physically improved while being physiologically compatible. Due to our two-step manufacturing technique, we avoided the requirement to raise the PCL matrix temperature prior to printing, while still ensuring a homogenous distribution of rGO. TheUltimately, high-fidelity, repeatable, and consistent 3D-printed scaffolds were the end product. A uniformly distributed sampleconsiderable gains in mechanical competency as a result of the PCL matrix rGO sheets and the build design. Re-stacking and aggregation of the rGO sheets inside the matrix led to the loss of mechanical characteristics when the rGO filler concentration was increased above 0.5 percent.

The inclusion of rGO had no negative cellular effects, and all scaffolds were shown to sustain stem cell growth and viability in vitro. Our 3D printed composite scaffolds are both structurally strengthened and physiologically friendly since we employed rGO as a filler in PCL, which is one of the most commonly used polymers in the production of scaffolds. Regenerative engineering of diverse tissues and organs may be facilitated by the PCL-rGO scaffolds proposed in this work.in the scaffolds' mechanical characteristics. Significantly improved the performance of the rGO, even in modest doses of 0.5 Wt.%.

Materials and methods

Preparation of the ink. Solvent evaporation film casting was used to make the 3D printing inks.At 0.5, 1 or 3 wt. % of reduced graphene oxide (rGO), Polysciences, Warrington, Pa., dissolved polycaprolactone in dichloromethane (DCM) and characterised.a suburb of St. Louis PCL or PCL + rGO had a weight of 1 g to 5 mL in DCM, depending on the formulation. While the mixes were being vortexed, they were kept atTemperature for three hours to achieve full PCL dissolution and homogeneous rGO dispersion. Preliminary Candidate List (PCL)To make the PCL-rGO composite films, solutions in 100 mm petri dishes were cast and then dried underovernight in the open air. After another 24 hours of lyophilization, the films were ready to be used. Finally, the movieswere sliced up into smaller pieces so that they could be fed into the 3D printer's cartridge (Fig. 1).

Scaffold 3D printing.

SolidWorks Version 2018, Dassault Systémes, Vélizy-Villacoublay, France, was used to design structures of various thicknesses and exported as STL files into the Perfactory RP software Version 3.0. (EnvisionTEC GmbH, Germany). Slices were made from the designs.a layer thickness of 300 m was used, with a 60° angle between each layer. The length of the strand and the diameter of the poreThey were set at 300 m for the first and 420 m for the second (the distance between two adjacent strands) (Fig. 3a).An extrusion-based 3D printer (4th Generation 3D Bioplotter, Manufacturer) was used to create the structures.A series from the German EnvisionTEC GmbH. The high-temperature stainless-steel cartridge was filled with this solution.using pellets, either pure PCL or a PCL-rGO hybrid. The temperature was then increased to 100 °C and maintained for a few minutes.during the length of the printing process. Prior to printing, the cartridge was heated to at least 100 °C for at least 20 minutes.check that the pellets are completely melted and that there are no air bubbles. The platform's temperature was carefully monitored and maintained.the whole operation was carried out at 10 °C. At 0.6 MPa, the pressure was applied, and the speed of the head's movement was increased toUse the G24 metallic nozzle to extrude the inks out of the cartridge. Set a 20-second delay between printing successive pages.layers to give the preceding ones enough time to solidify. After printing, the structures were easily accessiblecollected. Disposable punches were used to make cylindrical scaffolds from the structures.use. Scaffolds of 4 mm thickness x 4 mm diameter were used for mechanical testing and SEM imaging.Scaffolds with a thickness of 1 millimetre and diameter of 3 millimetres were used in all subsequent tests (Fig. 1). All the samplesafter printing, they were kept dry in vacuum desiccators.

Morphological characterization.

As well as taking pictures of each layer of the structure using the Bioplotter CCD camera, SEM was utilised to examine its morphological aspects.. Stainless-steel plates were used to attach the samples (n = 3 per group).A FEI Nova NanoSEM 450 was used to image the stubs, which were coated with gold–palladium and sputter-coated.5 mm in diameter and a 15 kV acceleration voltage are the specifications.The code inside each scaffold was used to quantify average diameter and average pore size of the individual strands.ImageJ71This is the 1.53c version (https://imagej.nh.gov/ij/). The first step in using this code is to choose a specific area of interest.A certain strand was chosen. The code was used to locate the boundaries of that strand. Lines that are perpendicular toTheprogramme estimated the distance from one side of the boundary to the other. For every strand, the average of these metricsthe strand's average length in inches (strand diameter). Until the average width was reached, this procedure was repeated several times.The average strand diameter of all strands across all SEM pictures was calculated (Fig. 3c). Values for the pore sizes were obtainedSimilarly, the area of interest is the breadth between each pair of neighbouringstrands.

Thermogravimetric analysis (TGA): Thermal analysis by use of a thermograph (TGA). Evaluation of the incorporation was done with the use of a TA Instruments TGA (TGA Q500).the scaffolds contain rGO. Using nitrogen as a

gas, TGA was carried out at temperatures ranging from ambient toto 600 ℃ in 10 minutes.

Xray powder diffraction (XRD): Powder diffraction using X-rays (XRD). the presence of rGO was determined by XRD (Bruker D2 Phaser)inside the framework of the scaffolds. X-ray diffraction was used to analyse the samples after they were placed on the corundum plates.2 = 10–60° range with a 0.01° step size.Evaluation of wettability For each sample, we measured the contact angle between water and air using the Dataphysicsinstrument.

Wettability assessment: The sessile drop technique and the OCA20 contact angle analyzer are both used at room temperature. Structural samples with a low densityA drop of deionized water was automatically applied to each one (n = 5) after they were 3D printed. Absorptive capacitycamera, and measurements were made using a high-speed framing camera.

Degradation behavior: As a result of degradation. Percentages were used to gauge how quickly the scaffolds degraded.When submerged in SBF for 14 days, the weight loss and swelling rates of the study groups were compared.SBF solution was created as previously published methods72 were followed.Simply, there are 7.996 g (NaHCO3), 0.350 g (NaCl)A total of 0.224 grammes of KCl, 0.22 grammes K2HPO4.3H2O and 0.228 grammes of KH2O.0.305 g of MgCl2.6H2O in waterIn 40 millilitres of 1 M-HCl, 0.27 gramme of CaCl2,0.071 grammes of sodium sulphateas well as 6.057 g of(Sigma) CH2OH)3CNH2 was dissolved in 1 litre of water in a stepwise fashion.of 36.5°C-controlled distilled water was used. 1–2 minutes after the addition of and the complete dissolution of the salts,In order to achieve a pH of 7.4, the final salt solution was acidified. The scaffolds' initial weights (n = 3 groups/time point)They were able to keep track of it. A 15 mL solution of 1 SBF was used to incubate the scaffolds, and they were maintained at room temperature throughout this time.Heating to 37 degrees Celsius. Every week, a new batch of the SBF solution was made. After three, seven, and fourteen days, the scaffolds were harvestedFor more evaluations.Structuralbehaviour was evaluated by putting the harvestable structures on filter paper under high pressure.vacuum for one minute before weighing them moist to get an idea of their mass. After 48 hours of freeze-drying, the scaffolds were ready to use.Dry weights were tallied and entered into a database. The percentage of growth was calculated using the following equation:

$$Swelling\ rate = \frac{W_w - W_d}{W_d} \times 100$$

There is a difference between the wet weight (Ww) and dry weight (Wd).The percentage of weight reduction was calculated using the following equation:

$$Weight\ loss = \frac{W_i - W_d}{W_i} \times 100$$

where Wi is the initial weight, and Wd is the dry weight.Mechanics education.

Mechanical studies: The Instron 5544 mechanical tester (Norwood, MA) with a 2 kN load cell was used to examine the scaffolds' mechanical characteristics. Scaffolds (n = 4) were exposed to 30 percent strain limit uniaxial compressive loading at crosshead speed of 2 mm/min.TheBluehillUniversal programme Version 3.61 was used to compute the results. The modulus of elasticity wasCompressive strength values were calculated using the 0.2 percent strain offset linear slope technique.based on a 20 percent strain

Wideangle Xray scattering (WAXS): Compressive stressX-ray scattering with a large field of view (WAXS). Oxford Diffraction was used to get the WAXS patternsOnyx CCD area detector with Cu-K radiation for the XCalibur PX Ultra (Concord, MA) The scavenging crates wereMeasurement was done across the range of zero to fifty utilising custom-built sample holders.At room temperature, a step size of 0.03 2 is used. CrysAlisPro software Version was used to gather and analyse the data.171.40.67a. The scattering vector's magnitude was determined using the following equation:

$$q = \left(\frac{4\pi}{\lambda}\right) sin\frac{\theta}{2}$$

where θ is the scattering angle and λ = 1.5418 Å is the X-ray wavelength for Cu-Kα.

In vitro studies: All cell culture reagents and human adipose-derived stem cells (hADSCs) were bought from Invitrogen (Carlsbad, CA). It was bought from Promega's CellTiter 96 Aqueous One Solution Cell Proliferation Assay (MTS) (Madison, WI). Grown on MesenPRO RS base medium with 0.5% glucose, the human ADSCsL-glutamine, penicillin/streptomycin, and a growth supplement of

MesenPRO RS were used in regular media changesA few times a week. TrypLE Express without phenol was used to remove the cells from the culture flasks at P2.centrifuged at 210g for 5 minutes and seeded onto sterile scaffolds that had been put in ultra-low attachmentPlates with 96 wells.

Following a 20-minute soak in 70 percent ethanol, the scaffolds were sterilised.30 minutes of UV exposure At a density of 50,000 cells/scaffold, the cells were planted in 5 L of medium and left to grow.should be attached to the scaffolds for one hour before the wells are filled with growth material;Assay that may be performed on either a living or deceased subject.

The LIVE/DEAD assay was used to determine if cells growing on 3D-printed scaffolds were still alive.During days 3, 7 and 14 of the experiment After being moved to fresh wells and rinsing twice with DPBS, the scaffolds were thenincubated for 15 minutes in a staining solution consisting of 10 mL DPBS, 5 L calcine AM, and 20 L ethidium homodimer-1.We used the Zeiss LSM Confocor2 at 10x magnification for our imaging.

AfterwardsFor all of the images, a 3D Median filter was applied to them using the ImageJ programme (version 1.53c)in order to limit the amount of noise generated by the pictures during the z-projection methodThe polymerization of PCL.Viability. The MTS was used to test the cell viability and proliferation on the 3D printed scaffolds.days 3, 7 and 14 are the days for testing. Transferred to fresh wells, rinsed once with DPBS, and resuspendedthen incubated for two hours at 37 °C with 30 L of MTS solution and 200 L of growth medium. TheA plate reader (BioTek, Inc.) was used to measure the samples' absorbance at 490 nm in triplicate.The Synergy H1 in Winooski, Vermont.

Statistical analysis: The use of scaffolds devoid of MTS reagent is necessary to avoid scaffold interference during the analysis.They employed cells and subtracted them from the absorbance values of cell-seeded structures. Each piece of informationMean absorbance values of the control PCL scaffolds were used to standardise the time point.cellular viability is the term used to describe this (percent of control).Analytical statistics. The mean and standard deviation are used to summarise all of the research findings (SD). StatisticalThe Holm-Sidak post hoc test and the Bonferroni post hoc test were used for one-way analysis of variance (one-way ANOVA) and two-way analysis of variance (two-way ANOVA). *p 0.05, **p 0.01; ***p 0.001; and ****p 0.0001 are considered significant.

Author contributions: SEM imaging and contact angle measurements; mechanical testing; cell assays; and help in all other experiments were carried out by A.S., and he prepared the text. L.D. planned the work, developed the experiments, and carried out the study, including scaffolding, as well.support with all additional investigations, including manufacturing, WAXS tests, and cellular assays, as well as writing and editingthe text that has been written down. SEM imaging, TGA, XRD, and other techniques were devised by M.B., and he carried out the study.the biodegradation research, cellular tests, and the support in all other experiments. J.R.aided in the mechanical testing and analysis. C.T.L. oversaw all aspects of the study. All writers made a contribution.to the debates over scientific theories. The final paper was approved by all of the writers.

References

1. Barajaa, M. A., Nair, L. S. & Laurencin, C. T. Bioinspired scaffold designs for regenerating musculoskeletal tissue interfaces. Regen.Eng. Transl. Med. https ://doi.org/10.1007/s4088 3-019-00132 -3 (2019).

2. Mabrouk, M., Beherei, H. H. & Das, D. B. Recent progress in the fabrication techniques of 3D scaffolds for tissue engineering.Mater. Sci. Eng. C https ://doi.org/10.1016/j.msec.2020.11071 6 (2020).

3. Wheelton, A., Mace, J., Khan, W. & Anand, S. Biomaterials and fabrication to optimise scaffold properties for musculoskeletaltissue engineering. Curr. Stem Cell Res. Therapy 11, 578–584. https ://doi.org/10.2174/15748 88x11 66616 06141 01037 (2016).

4. Mirdamadi, E. S., Kalhori, D., Zakeri, N., Azarpira, N. &Solati-Hashjin, M. Liver tissue engineering as an emerging alternativefor liver disease treatment. Tissue Eng. Part B Rev. 26, 145–163. https ://doi.org/10.1089/ten.teb.2019.0233 (2020).

5. Sola, A. et al. Development of solvent-casting particulate leaching (SCPL) polymer scaffolds as improved three-dimensional supportsto mimic the bone marrow niche. Mater. Sci. Eng. C 96, 153–165. https ://doi.org/10.1016/j.msec.2018.10.086 (2019).

6. Nematollahi, Z. et al. Fabrication of chitosan silk-based tracheal scaffold using freeze-casting method. Iran. Biomed. J. 21, 228–239.https ://doi.org/10.18869 /acadp ub.ibj.21.4.228 (2017).

7. Tohamy, K. M., Mabrouk, M., Soliman, I. E., Beherei, H. H. &Aboelnasr, M. A. Novel alginate/hydroxyethyl cellulose/hydroxyapatitecomposite scaffold for bone regeneration: in vitro cell viability and proliferation of human mesenchymal stem cells. Int. J. Biol.Macromol. 112, 448–460. https ://doi.org/10.1016/j.ijbio mac.2018.01.181 (2018).

8. Hasani-Sadrabadi, M. M. et al. Hierarchically patterned polydopamine-containing membranes for periodontal tissue engineering.ACS Nano 13, 3830–3838. https ://doi.org/10.1021/acsna no.8b096 23 (2019).

9. Gögele, C. et al. Enhanced growth of lapine anterior cruciate ligament-derived fibroblasts on scaffolds embroidered from poly(llactide-co-ε-caprolactone) and polylactic acid threads functionalized by fluorination and hexamethylene diisocyanate cross-linkedcollagen foams. Int. J. Mol. Sci. https ://doi.org/10.3390/ijms2 10311 32 (2020).

10. Xie, Y. et al. High-performance porous polylactide stereocomplex crystallite scaffolds prepared by solution blending and saltleaching. Mater. Sci. Eng. C 90, 602–609. https ://doi.org/10.1016/j.msec.2018.05.023 (2018).

11. Mao, D., Li, Q., Li, D., Tan, Y. & Che, Q. 3D porous poly(ε-caprolactone)/58S bioactive glass–sodium alginate/gelatin hybrid scaffoldsprepared by a modified melt molding method for bone tissue engineering. Mater. Des. 160, 1–8. https ://doi.org/10.1016/j.matde s.2018.08.062 (2018).

12. Chen, P. et al. Preparation and characterization of poly(L-lactide-co-glycolide-co-ε-caprolactone) scaffolds by thermally inducedphase separation. J. Macromol. Sci. Part B https ://doi.org/10.1080/00222 348.2020.17351 36 (2020).

13. Basu, A., Rothermund, K., Ahmed, M. N. & Syed-Picard, F. N. Self-assembly of an organized cementum-periodontal ligament-likecomplex using scaffold-free tissue engineering. Front. Physiol. https ://doi.org/10.3389/fphys .2019.00422 (2019).

14. Kascholke, C. et al. Biodegradable and adjustable sol-gel glass based hybrid scaffolds from multi-armed oligomeric building blocks.ActaBiomater. 63, 336–349. https ://doi.org/10.1016/j.actbi o.2017.09.024 (2017).

15. Chiesa, I. et al. Endothelial cells support osteogenesis in an in vitro vascularized bone model developed by 3D bioprinting. Biofabricationhttps ://doi.org/10.1088/1758-5090/ab6a1 d (2020).

16. Woodfield, T. et al. Biofabrication in tissue engineering. Comprehens. Biomater. 5(14), 236–266 (2017).

17. Matai, I., Kaur, G., Seyedsalehi, A., McClinton, A. & Laurencin, C. T. Progress in 3D bioprinting technology for tissue/organregenerative engineering. Biomaterialshttps ://doi.org/10.1016/j.biomateria ls.2019.11953 6 (2020).

18. Shuai, C. et al. A strawberry-like Ag-decorated barium titanate enhances piezoelectric and antibacterial activities of polymerscaffold. Nano Energy https ://doi.org/10.1016/j.nanoe n.2020.10482 5 (2020).

19. Yang, Y. et al. Metal organic frameworks as a compatible reinforcement in a biopolymer bone scaffold. Mater. Chem. Front. 4,973–984. https ://doi.org/10.1039/c9qm0 0772e (2020).

20. Placone, J. K. & Engler, A. J. Recent advances in extrusion-based 3D printing for biomedical applications. Adv. Healthcare Mater.https ://doi.org/10.1002/adhm.20170 1161 (2018).

21. Ogueri, K. S., Jafari, T., Escobar Ivirico, J. L. & Laurencin, C. T. Polymeric biomaterials for scaffold-based bone regenerative engineering.Regen. Eng. Transl. Med. 5, 128–154. https ://doi.org/10.1007/s4088 3-018-0072-0 (2019).

22. Guo, Y., Liang, K. & Ji, Y. New degradable composite elastomers of POC/PCL fabricated via in-situ copolymerization blendingstrategy. Eur. Polymer J. 110, 337–343. https ://doi.org/10.1016/j.eurpo lymj.2018.11.048 (2019).

23. Espinoza, S. M., Patil, H. I., San Martin Martinez, E., Casañas Pimentel, R. & Ige, P. P. Poly-ε-caprolactone (PCL), a promisingpolymer for pharmaceutical and biomedical applications: Focus on nanomedicine in cancer. Int. J. Polym. Mater. Polym. Biomater.69, 85–126. https ://doi.org/10.1080/00914 037.2018.15399 90 (2019).

24. Teoh, S.-H., Goh, B.-T. & Lim, J. Three-dimensional printed polycaprolactone scaffolds for bone regeneration success and futureperspective. Tissue Eng. Part A 25, 931–935. https ://doi.org/10.1089/ten.tea.2019.0102 (2019).

25. Laurencin, C. T. &Daneshmandi, L. Graphene for regenerative engineering. Int. J. Ceram. Eng. Sci. 2, 140–143. https ://doi.org/10.1002/ces2.10045 (2020).

26. Allen, M. J., Tung, V. C. &Kaner, R. B. Honeycomb carbon: A review of graphene. Chem. Rev. 110, 132–145. https ://doi.org/10.1021/cr900 070d (2010).

27. Daneshmandi, L., Barajaa, M., Tahmasbi Rad, A., Sydlik, S. A. & Laurencin, C. T. Graphene-based biomaterials for bone regenerativeengineering: A comprehensive review of the field and considerations regarding biocompatibility and biodegradation. Adv.Healthcare Mater. https ://doi.org/10.1002/adhm.20200 1414 (2020).

28. Chen, D., Feng, H. & Li, J. Graphene oxide: Preparation, functionalization, and electrochemical applications. Chem. Rev. 112,6027–6053. https ://doi.org/10.1021/cr300 115g (2012).

29. Shuai, C. et al. A graphene oxide-Ag co-dispersing nanosystem: Dual synergistic effects on antibacterial activities and mechanicalproperties of polymer scaffolds. Chem. Eng. J. 347, 322–333. https ://doi.org/10.1016/j.cej.2018.04.092 (2018).

30. Reina, G. et al. Promises, facts and challenges for graphene in biomedical applications. Chem. Soc. Rev. 46, 4400–4416. https ://doi.org/10.1039/c7cs0 0363c (2017).

31. Chakraborty, S., Ponrasu, T., Chandel, S., Dixit, M. &Muthuvijayan, V. Reduced graphene oxide-loaded nanocomposite scaffoldsfor enhancing angiogenesis in tissue engineering applications. R. Soc. Open Sci. https ://doi.org/10.1098/rsos.17201 7 (2018).

32. Marrella, A. et al. "Green-reduced" graphene oxide induces in vitro an enhanced biomimetic mineralization of polycaprolactoneelectrospun meshes. Mater. Sci. Eng., C 93, 1044–1053. https ://doi.org/10.1016/j.msec.2018.08.052 (2018).

33. Correa, E., Moncada, M. E., Gutiérrez, O. D., Vargas, C. A. & Zapata, V. H. Characterization of polycaprolactone/rGOnanocompositescaffolds obtained by electrospinning. Mater. Sci. Eng. C https ://doi.org/10.1016/j.msec.2019.10977 3 (2019).

34. Angulo-Pineda, C. et al. Electroactive 3D printed scaffolds based on percolated composites of polycaprolactone with thermallyreduced graphene oxide for antibacterial and tissue engineering applications. Nanomaterialshttps ://doi.org/10.3390/nano1 0030428 (2020).

35. Vijayavenkataraman, S., Thaharah, S., Zhang, S., Lu, W. F. &Fuh, J. Y. H. 3D-printed PCL/rGO conductive scaffolds for peripheralnerve injury repair. Artif. Organs 43, 515–523. https ://doi.org/10.1111/aor.13360 (2018).

36. Rehman, S. R. et al. Reduced graphene oxide incorporated GelMA hydrogel promotes angiogenesis for wound healing applications.Int. J. Nanomed. 14, 9603–9617. https ://doi.org/10.2147/ijn.S2181 20 (2019).

37. Kosowska, K., Domalik-Pyzik, P., Krok-Borkowicz, M. &Chłopek, J. Synthesis and characterization of chitosan/reduced grapheneoxide hybrid composites. Materials https ://doi.org/10.3390/ma121 32077 (2019).

38. Nalvuran, H., Elçin, A. E. &Elçin, Y. M. Nanofibrous silk fibroin/reduced graphene oxide scaffolds for tissue engineering and cellculture applications. Int. J. Biol. Macromol. 114, 77–84. https ://doi.org/10.1016/j.ijbio mac.2018.03.072 (2018).

39. MehendaleSaahil, V., Mellor Liliana, F., Taylor Michael, A., Loboa Elizabeth, G. &Shirwaiker Rohan, A. Effects of 3D-bioplottedpolycaprolactone scaffold geometry on human adipose-derived stem cell viability and proliferation. Rapid Prototyp. J. 23, 534–542.https ://doi.org/10.1108/RPJ-03-2016-0035 (2017).

40. Hutmacher, D. W. et al. Mechanical properties and cell cultural response of polycaprolactone scaffolds designed and fabricated viafused deposition modeling. J. Biomed. Mater. Res. 55, 203–216. https ://doi.org/10.1002/1097-4636(20010 5)55:2%3c203 ::Aid-jbm1007%3e3.0.Co;2-7 (2001).

41. Lee, J.-S. et al. Effect of pore architecture and stacking direction on mechanical properties of solid freeform fabrication-basedscaffold for bone tissue engineering. J. Biomed. Mater. Res., Part A 100A, 1846–1853. https ://doi.org/10.1002/jbm.a.34149 (2012).

42. Zein, I., Hutmacher, D. W., Tan, K. C. & Teoh, S. H. Fused deposition modeling of novel scaffold architectures for tissue engineeringapplications. Biomaterials 23, 1169–1185. https ://doi.org/10.1016/s0142 -9612(01)00232 -0 (2002).

43. Chen, G. & Kawazoe, N. Preparation of polymer scaffolds by ice particulate method for tissue engineering. Biomater. Nanoarchitecton.3(1), 77–95 (2016).

44. Yuk, H. & Zhao, X. A new 3D printing strategy by harnessing deformation, instability, and fracture of viscoelastic inks. Adv. Mater.https ://doi.org/10.1002/adma.20170 4028 (2018).

45. Wang, K. Die swell of complex polymeric systems. Viscoelast. Theory Biol. Appl. 1, 77–96 (2012).

46. Feng, B. et al. The effect of pore size on tissue ingrowth and neovascularization in porous bioceramics of controlled architecturein vivo. Biomed. Mater. https ://doi.org/10.1088/1748-6041/6/1/01500 7 (2011).

47. Akita, K. et al. Fabrication of porous carbonate apatite granules using microfiber and its histological evaluations in rabbit calvarialbone defects. J. Biomed. Mater. Res. Part A 108, 709–721. https ://doi.org/10.1002/jbm.a.36850 (2019).

48. Fadaie, M. & Mirzaei, E. Nanofibrillated chitosan/polycaprolactone bionanocomposite scaffold with improved tensile strengthand cellular behavior. Nanomed. J. 5, 77–89 (2018).

49. Soomro, S. A., Gul, I. H., Naseer, H., Marwat, S. & Mujahid, M. Improved performance of CuFe2O4/rGO nanohybrid as an anodematerial for lithium-ion batteries prepared via facile one-step method. Curr. Nanosci. 15, 420–429. https ://doi.org/10.2174/1573413714 66618 11151 22016 (2019).

50. Wang, W. et al. Morphological, mechanical and biological assessment of PCL/pristine graphene scaffolds for bone regeneration.Int. J. Bioprint. https ://doi.org/10.18063 /ijb.2016.02.009 (2016).

51. Safikhani, M. M., Zamanian, A. &Ghorbani, F. Synergistic effects of retinoic acid and graphene oxide on the physicochemicaland in-vitro properties of electrospun polyurethane scaffolds for bone tissue engineering. e-Polymers 17, 363–371. https ://doi.org/10.1515/epoly -2016-0304 (2017).

52. Zhang, et al. Fabrication and application of novel porous scaffold in situ-loaded graphene oxide and osteogenic peptide by cryogenic3D printing for repairing critical-sized bone defect. Moleculeshttps ://doi.org/10.3390/molec ules2 40916 69 (2019).

53. Esmaeili, E. et al. The biomedical potential of cellulose acetate/polyurethane nanofibrous mats containing reduced grapheneoxide/silver nanocomposites and curcumin: Antimicrobial performance and cutaneous wound healing. Int. J. Biol. Macromol.152, 418–427. https ://doi.org/10.1016/j.ijbio mac.2020.02.295 (2020).

54. Lee, C.-S., Yu, S. & Kim, T. One-step electrochemical fabrication of reduced graphene oxide/gold nanoparticles nanocompositemodifiedelectrode for simultaneous detection of dopamine, ascorbic acid, and uric acid. Nanomaterialshttps ://doi.org/10.3390/nano8 01001 7 (2017).

55. Abbandanak, S. N. H. et al. Morphological/SAXS/WAXS studies on the electrochemical synthesis of graphene nanoplatelets.Ceram. Int. 45, 20882–20890. https ://doi.org/10.1016/j.ceram int.2019.07.077 (2019).

56. Hofmann, D., Keinath, M., Thomann, R. &Mülhaupt, R. Thermoplastic carbon/polyamide 12 composites containing functionalizedgraphene, expanded graphite, and carbon nanofillers. Macromol. Mater. Eng. 299, 1329–1342. https ://doi.org/10.1002/mame.201400066 (2014).

57. Shuai, C. et al. Graphene oxide reinforced poly(vinyl alcohol): Nanocomposite scaffolds for tissue engineering applications. RSCAdv. 5, 25416–25423. https ://doi.org/10.1039/c4ra1 6702c (2015).

58. Wan, C. & Chen, B. Poly(ε-caprolactone)/graphene oxide biocomposites: Mechanical properties and bioactivity. Biomed. Mater.https ://doi.org/10.1088/1748-6041/6/5/05501 0 (2011).

59. Papageorgiou, D. G., Kinloch, I. A. & Young, R. J. Mechanical properties of graphene and graphene-based nanocomposites. Prog.Mater Sci. 90, 75–127. https ://doi.org/10.1016/j.pmats ci.2017.07.004 (2017).

60. Dizon, J. R. C., Espera, A. H., Chen, Q. &Advincula, R. C. Mechanical characterization of 3D-printed polymers. Addit. Manuf.20, 44–67. https ://doi.org/10.1016/j.addma .2017.12.002 (2018).

61. Olate-Moya, F. et al. Chondroinductive alginate-based hydrogels having graphene oxide for 3D printed scaffold fabrication. ACSAppl. Mater. Interfaces. 12, 4343–4357. https ://doi.org/10.1021/acsam i.9b220 62 (2020).

62. Zhou, X. et al. 3D bioprinted graphene oxide-incorporated matrix for promoting chondrogenic differentiation of human bonemarrow mesenchymal stem cells. Carbon 116, 615–624. https ://doi.org/10.1016/j.carbo n.2017.02.049 (2017).

63. Chen, Q. et al. 3D printing biocompatible polyurethane/poly(lactic acid)/graphene oxide nanocomposites: Anisotropic properties.ACS Appl. Mater. Interfaces. 9, 4015–4023. https ://doi.org/10.1021/acsam i.6b117 93 (2017).

64. Choe, G., Oh, S., Seok, J. M., Park, S. A. & Lee, J. Y. Graphene oxide/alginate composites as novel bioinks for three-dimensionalmesenchymal stem cell printing and bone regeneration applications. Nanoscale 11, 23275–23285. https ://doi.org/10.1039/c9nr07643c (2019).

65. Liu, S., Bastola, A. K. & Li, L. A 3D printable and mechanically robust hydrogel based on alginate and graphene oxide. ACS Appl.Mater. Interfaces. 9, 41473–41481. https ://doi.org/10.1021/acsam i.7b135 34 (2017).

66. Unagolla, J. M. & Jayasuriya, A. C. Enhanced cell functions on graphene oxide incorporated 3D printed polycaprolactone scaffolds.Mater. Sci. Eng. C 102, 1–11. https ://doi.org/10.1016/j.msec.2019.04.026 (2019).

67. Holt, B. D., Arnold, A. M. &Sydlik, S. A. In It for the long Haul: The cytocompatibility of aged graphene oxide and its degradationproducts. Adv. Healthc. Mater. 5, 3056–3066. https ://doi.org/10.1002/adhm.20160 0745 (2016).

68. Arnold, A. M., Holt, B. D., Daneshmandi, L., Laurencin, C. T. &Sydlik, S. A. Phosphate graphene as an intrinsically osteoinductivescaffold for stem cell-driven bone regeneration. Proc. Natl. Acad. Sci. U.S.A. 116, 4855–4860. https ://doi.org/10.1073/pnas.1815434116 (2019).

69. Arnold, A. M., Holt, B. D., Sydlik, S. A., Laurencin, C. T. &Daneshmandi, L. Phosphate functionalized graphene oxide based bonescaffolds. US patent (2020).

70. Lee, W. C. et al. Origin of enhanced stem cell growth and differentiation on graphene and graphene oxide. ACS Nano 5, 7334–7341.https ://doi.org/10.1021/nn202 190c (2011).

71. Bickford, J. R. Automatic stripe analysis tool. (ARMY RESEARCH LAB ADELPHI MD SENSORS AND ELECTRON DEVICESDIRECTORATE, 2013).

72. Kokubo, T., Kushitani, H., Sakka, S., Kitsugi, T. &Yamamuro, T. Solutions able to reproducein vivo surface-structure changes inbioactive glass-ceramic A-W3. J. Biomed. Mater. Res. 24, 721–734. https ://doi.org/10.1002/jbm.82024 0607 (1990).

73. Jiang, T. et al. Chitosan–poly(lactide-co-glycolide) microsphere-based scaffolds for bone tissue engineering: In vitro degradationand in vivo bone regeneration studies. Acta Biomater. 6, 3457–3470. https ://doi.org/10.1016/j.actbi o.2010.03.023 (2010).